Refractometer based on fiber Bragg grating Fabry-Pérot cavity embedded with a narrow microchannel

Kaiming Zhou,* Zhijun Yan, Lin Zhang, and Ian Bennion

Photonic Research Group, Aston University, Birmingham B4 7ET, United Kingdom
**k.zhou@aston.ac.uk*

Abstract: We report on inscription of microchannels of different widths in optical fiber using femtosecond (fs) laser inscription assisted chemical etching and the narrowest channel has been created with a width down to only 1.2μm. Microchannels with 5μm and 35μm widths were fabricated together with Fabry-Pérot (FP) cavities formed by UV laser written fiber Bragg gratings (FBGs), creating high function and linear response refractometers. The device with a 5μm microchannel has exhibited a refractive index (RI) detection range up to 1.7, significantly higher than all fiber grating RI sensors. In addition, the microchannel FBG FP structures have been theoretically simulated showing excellent agreement with experimental measured characteristics.

OCIS codes: (060.2370) Fiber optics sensors; (120.2230) Fabry-Pérot; (160.2750) Glass and other amorphous materials.

References and links

1. K. M. Davis, K. Miura, N. Sugimoto, and K. Hirao, "Writing waveguides in glass with a femtosecond laser," Opt. Lett. **21**(21), 1729–1731 (1996).
2. Y. Cheng, K. Sugioka, K. Midorikawa, M. Masuda, K. Toyoda, M. Kawachi, and K. Shihoyama, "Control of the cross-sectional shape of a hollow microchannel embedded in photostructurable glass by use of a femtosecond laser," Opt. Lett. **28**(1), 55–57 (2003).
3. K. Zhou, Y. Lai, X. Chen, K. Sugden, L. Zhang, and I. Bennion, "A refractometer based on a micro-slot in a fiber Bragg grating formed by chemically assisted femtosecond laser processing," Opt. Express **15**(24), 15848–15853 (2007).
4. S. Mihailov, C. Smelser, D. Grobnic, R. Walker, P. Lu, H. Ding, and J. Unruh, "Bragg gratings written in all-SiO2 and Ge-doped core fibers with 800-nm femtosecond radiation and a phase mask," J. Lightwave Technol. **22**(1), 94–100 (2004).
5. A. Martinez, I. Y. Khrushchev, and I. Bennion, "Direct inscription of Bragg gratings in coated fibers by an infrared femtosecond laser," Opt. Lett. **31**(11), 1603–1605 (2006).
6. Y. Lai, K. Zhou, K. Sugden, and I. Bennion, "Point-by-point inscription of first-order fiber Bragg grating for C-band applications," Opt. Express **15**(26), 18318–18325 (2007).
7. G. D. Marshall, R. J. Williams, N. Jovanovic, M. J. Steel, and M. J. Withford, "Point-by-point written fiber-Bragg gratings and their application in complex grating designs," Opt. Express **18**(19), 19844–19859 (2010).
8. Y. Kondo, K. Nouchi, T. Mitsuyu, M. Watanabe, P. G. Kazansky, and K. Hirao, "Fabrication of long-period fiber gratings by focused irradiation of infrared femtosecond laser pulses," Opt. Lett. **24**(10), 646–648 (1999).
9. T. Wei, Y. Han, Y. Li, H.-L. Tsai, and H. Xiao, "Temperature-insensitive miniaturized fiber inline Fabry-Perot interferometer for highly sensitive refractive index measurement," Opt. Express **16**(8), 5764–5769 (2008).
10. Y. Wang, D. N. Wang, M. Yang, W. Hong, and P. Lu, "Refractive index sensor based on a microhole in single-mode fiber created by the use of femtosecond laser micromachining," Opt. Lett. **34**(21), 3328–3330 (2009).
11. Y. Wang, M. Yang, D. N. Wang, S. Liu, and P. Lu, "Fiber in-line Mach-Zehnder interferometer fabricated by femtosecond laser micromachining for refractive index measurement with high sensitivity," J. Opt. Soc. Am. B **27**(3), 370–374 (2010).
12. Z. Ran, Y. Rao, J. Zhang, Z. Liu, and B. Xu, "A miniature fiber-optic refractive-index sensor based on laser-machined Fabry–Perot interferometer tip," J. Lightwave Technol. **27**(23), 5426–5429 (2009).
13. R. Taylor, C. Hnatovsky, and E. Simova, "Applications of femtosecond laser induced self-organized planar nanocracks inside fused silica glass," Laser Photonics Rev. **2**(1-2), 26–46 (2008).
14. K. J. Vahala, "Optical microcavities," Nature **424**(6950), 839–846 (2003).

#141693 - $15.00 USD Received 25 Jan 2011; revised 11 Mar 2011; accepted 24 Mar 2011; published 2 Jun 2011

15. P. R. Villeneuve, J. S. Foresi, J. Ferrera, E. R. Thoen, G. Steinmeyer, S. Fan, J. D. Joannopoulos, L. C. Kimerling, H. I. Smith, and E. P. Ippen, "Photonic-bandgap microcavities in optical waveguides," Nature **390**(6656), 143–145 (1997).
16. A. Muller, E. B. Flagg, J. R. Lawall, and G. S. Solomon, "Ultrahigh-finesse, low-mode-volume Fabry-Perot microcavity," Opt. Lett. **35**(13), 2293–2295 (2010).
17. Y. Lai, K. Zhou, L. Zhang, and I. Bennion, "Microchannels in conventional single-mode fibers," Opt. Lett. **31**(17), 2559–2561 (2006).
18. J. Petrovic, Y. Lai, and I. Bennion, "Numerical and experimental study of microfluidic devices in step-index optical fibers," Appl. Opt. **47**(10), 1410–1416 (2008).
19. K. Zhou, X. Chen, G. Simpson, D. Zhao, L. Zhang, and I. Bennion, "Temperature referenced high sensitivity point-probe optical fiber chem-sensors based on cladding etched fiber bragg gratings," in *Optical Sensing*, B. Culshaw, A. Mignani, and R. Riesenberg, eds., **5459**, 409–414 (2004).
20. R. Kashyap, *Fiber Bragg Grating* (Academic Press, 1999).
21. S. Yuan and N. A. Riza, "General formula for coupling-loss characterization of single-mode fiber collimators by use of gradient-index rod lenses," Appl. Opt. **38**(15), 3214–3222 (1999).

1. Introduction

Refractometers are widely used in many industrial sectors, including food, beverage, environment, chemical and medical analysis etc. Traditional refractometers are based on bulky optics and have limitations for remote, in situ, miniaturized and high sensitive sensing. Optical fiber refractometers, on the other hand, have better merits in these terms. A number of fiber structures have been exploited for refractometers, including Fabry-Pérot (FP) cavity, tapered fiber and fiber gratings. Recently, the advancement of micromachining using femtosecond (fs) laser has provided a powerful tool for fabrication of microstructure devices for various applications, including refractive index (RI) measurement. One of the advantages of this technique is that the modification to materials relies on a nonlinear absorption of highly intense light above a threshold, which can be achieved with a focused fs laser beam. The modification can thus be made deep within the material and 3-dimensional (3D) structures can be created by scanning the laser beam. Researchers have implemented a range of novel photonic devices by fs laser inscription, including optical waveguides [1], microfluidic channels [2,3], fiber Bragg gratings (FBGs) [4–7] and long period gratings [8].

Micromachined hollow structures by fs laser in optical fiber have also been demonstrated for sensing applications since they allow infusion of surrounding substances (usually liquid or gas) to the fiber-core region wherein light propagates. An FP cavity was fabricated by ablating the fiber from its side and more than half of the fiber material was removed in the device section, leaving the device considerably fragile [9]. In [10,11], microholes were drilled directly through the fiber using laser ablation as well but the size of the hole is nonuniform through its depth and the wall is unevenly finished, introducing considerable scattering loss. Nevertheless, based on such micromachined hollow structures, a range of miniature sensors have been realized and most of them utilize an FP cavity only [9–12]. However, for RI sensing, especially for those close to the index of fiber glass, visibility of FP resonances diminishes due to the low reflectivity at the glass-liquid interface, giving rise to difficulty for data processing and limited operational RI range. Special coating process was introduced to overcome such a problem, but with increased complexity to the fabrication [12]. Our previous work has shown RI detection of liquid by employing a liquid core FBG based on a microchannel in the fiber and demonstrated a high sensitivity [3], however, the coupling from the normal fiber into the microchannel section (liquid core) is of high loss, thus degrading the signal. The other disadvantage of such a device is that its RI sensing exhibited a highly nonlinear response.

Compared to direct ablation using the high power fs laser, chemical etching assisted by low power fs laser inscription offers a number of advantages, including ultra-fine finishing surface, high flexibility and enhanced resolution. Since the interaction of the fs laser with materials is a highly nonlinear absorption, sub-wavelength structures can be produce [13]. An interesting device structure that could be implemented is an optical microcavity [14,15], which can find potential application in quantum optics and photonics [16]. In this paper, we

#141693 - $15.00 USD Received 25 Jan 2011; revised 11 Mar 2011; accepted 24 Mar 2011; published 2 Jun 2011

report microchannels of different widths engraved in optical fiber using such a method and the narrowest width down to only 1.2μm has been demonstrated. We also report the theoretical and experimental investigation of RI sensing characteristics of the proposed FBG FP cavities incorporating microchannels of different widths.

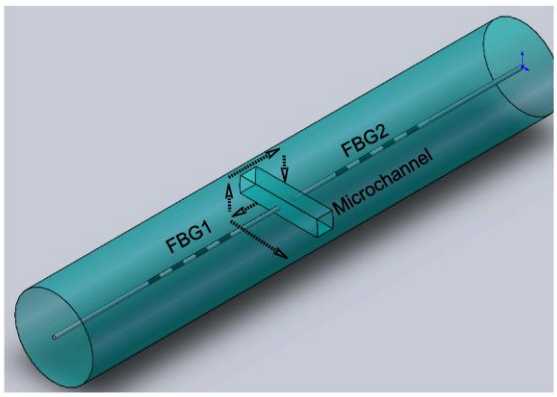

(a)

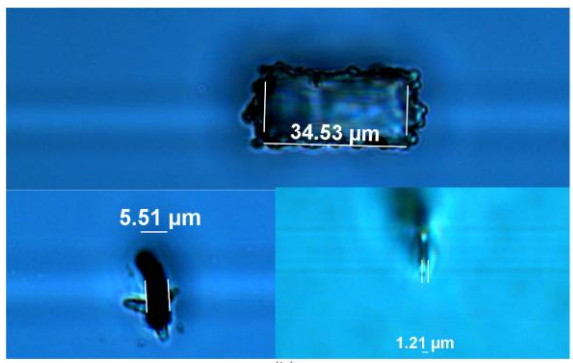

(b)

Fig. 1. (a) Schematic of the microchannel FBG FP device; the dashed arrow lines give the movement of the focal spot of the laser within the optical fiber. (b) Images of the fs laser inscription/chemical etching induced microchannels.

#141693 - $15.00 USD Received 25 Jan 2011; revised 11 Mar 2011; accepted 24 Mar 2011; published 2 Jun 2011

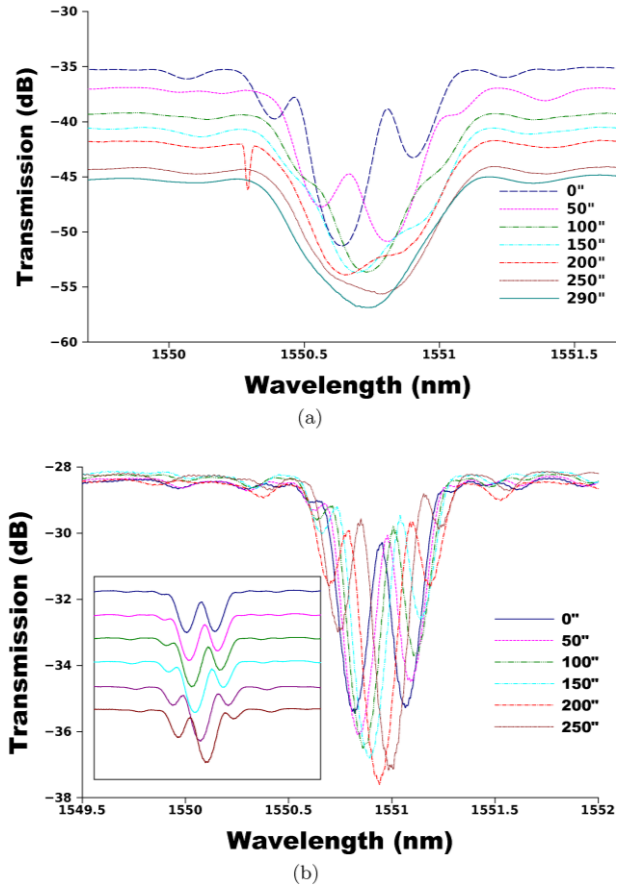

Fig. 2. Spectral evolution of the FBG FP cavity during the etching process with a (a) 35μm and (b) 5μm microchannel. Inset in (b) shows the offset spectra.

2. Device fabrication

Figure 1(a) is the schematic of the designed microchannel FBG FP device, which consists of an FP cavity formed by a pair of FBGs with a certain separation. In our design, two 2mm-long FBGs with the central wavelength at ~1551nm and reflectivity about 3dB were UV inscribed into the fiber with an estimated index modulation of 2×10^{-4}. The length of the FP cavity which is the separation between the two FBGs is about 1mm and in the middle of the cavity, a microchannel is induced by fs laser inscription assisted chemical etching technique as described in [3,17]. The fabrication process of the microchannel involves two main steps: (1) Inscription of the desired structure into the fiber by using a tightly focused fs laser beam; (2) Etching the fiber in a solution of 5% hydrofluoric acid (HF) for selective removal of the fs laser modified region. In the laser inscription process, the fiber was mounted on a dual-axes air-bearing translation stage, so that the desired structure could be written by moving the fiber with respect to the fs laser beam. Superior to direct ablation, this method relies on much lower laser energies to inscribe ultra-fine 3D pattern within the material, offering a much more enhanced resolution, precision and flexibility.

For microchannel inscription, a queue of shapes of the same geometry are inscribed and stacked across the cross section of the fiber, as illustrated by the dashed lines in Fig. 1(a). The shape can be arbitrarily chosen but a rectangle or a line is mostly suitable for microchannel inscription. The thickness of each layer is dependent on the energy and the scanning speed of

#141693 - $15.00 USD Received 25 Jan 2011; revised 11 Mar 2011; accepted 24 Mar 2011; published 2 Jun 2011

the laser and the inscribed layers need to overlap to create a continuous modification across the depth of the channel, allowing for a total removal of the inscribed structure by the etching. In our previous work [3], a microslot horizontally engraved along the axis of the fiber yielded significant loss, which was theoretically verified in [18]. In this work, however, we created microchannels of different widths along the fiber axis, but with the same height of 10μm, which is slightly larger than the diameter of the fiber core, so that the wave front of the light is not distorted and scattered greatly when propagating in the channel region. For the investigation, we have created microchannels of three different widths – 1.2μm, 5μm and 35μm and the latter two were embedded in FBG FP structures. For the inscription, only 90nJ fs pulse energy was used to inscribe 1.2μm microchannel but increased to 200nJ to inscribe 5μm and 35μm channels.

After the laser inscription, the fiber was chemically etched in a $_5$% HF solution for 15 minutes assisted by an ultrasonic bath to facilitate removal of the etching products from the fs laser inscribed region in the fiber. Figure 1(b) shows the images of the three microchannels after etching process. During the etching process, the transmission spectrum of the device was monitored to view the microchannel induced change. In the first 8 ~ 9 minutes, the spectrum showed no obvious change since the etching had not reached the core region yet. With etching carrying on, resonant peaks of the FP cavity began to shift to longer wavelength side. Figure 2 gives the spectral evolution of the two FBG FP devices with a 5μm and a 35μm channel. After 15 minutes of etching, the spectrum became stable, indicating that the entire modified region had been removed. Then, the fiber was taken out from the HF solution and rinsed with water. The FP resonant peaks were well reserved for the 5μm microchannel device, but almost disappear for the 35μm structure at the end of the etching. From the spectral evolution shown in Fig. 2, it can be seen that the microchannel induced a low overall insertion loss of ~0.13dB for the narrow channel but a much high loss of ~9.8dB for the wide channel sample. Because the loss is high, the FP resonances of the 35μm channel device were greatly suppressed, showing a poor visibility.

3. Refractive index sensing

The fabricated microchannel FBG FP devices were then subjected to a series of index oils (from Cargille) to measure their response to RI. After each measurement, the device was rinsed with acetone to remove the residual oil left in the microchannel till the original spectrum in air was restored. The response time is mainly dependent on the time for the liquid to infuse into the microchannel, which was almost instantaneously as observed during the measurement. The resonances in the spectrum are the interfering fringes of the FP cavity, which change in accordance with the phase shift of the electromagnetic field in the cavity due to the variation of RI of the oil. Figure 3(a) shows the spectral evolution of the 5μm microchannel sample with increasing RI. It can be immediately seen from the figure that once the oil is infused into the microchannel, the transmission loss decreases by 2.1dB and visibility of FP resonances increase inside of the Bragg reflection band. With increasing of RI, the FP resonant peaks shift obviously from the shorter to longer wavelength side and eventually move out of the Bragg reflection band, but subsequently, new peaks are regenerated from the shorter wavelength side. We can also see that the strength of the peak changes during its shifting and the deepest resonance occurs near the center of the Bragg reflection band. The relation of the peak wavelength with respect to RI for the 5μm microchannel FBG FP is given in Fig. 3(b), showing a linear trend with an RI sensitivity about 1.1nm/RIU (refractive index unit). Noticeablely, this narrow microchannel FBG FP device can detect RI change up to 1.7, which is remarkably higher than all fiber grating based refractometers, as the latter cannot exceed a range higher than the fiber core index around 1.44 [19].

For the 35μm microchannel device, the RI characterization was carried out for a much smaller RI range from 1.43 to 1.49, as the measureable FP resonances only existed in this

#141693 - $15.00 USD Received 25 Jan 2011; revised 11 Mar 2011; accepted 24 Mar 2011; published 2 Jun 2011

range due to high loss. The spectral evolution over the measured RI range is given in Fig. 4(a). The air caused transmission loss for this sample is much higher and in an order of ~22dB, as shown by the left figure in Fig. 4(a). Different from the 5μm microchannel sample shown in Fig. 3, this device shows no FP resonant peaks within the Bragg reflection band initially and only when the RI increased to 1.43, the FP resonant peaks start to occur and shift with increasing RI. Figure 4(b) plots the wavelength shift of one of the resonant peaks with RI change from 1.43 to 1.49, which also exhibits a good linear response. Although the detection range is much more reduced for this 35μm microchannel sample, the RI sensitivity is significantly high, reaching a value of 9nm/RIU compared to only 1.1nm/RIU from the 5μm channel device. However, with further increasing of RI above 1.49, the FP resonant peaks diminish, indicating the resurrection of loss due to index mismatching between the liquid and the fiber core.

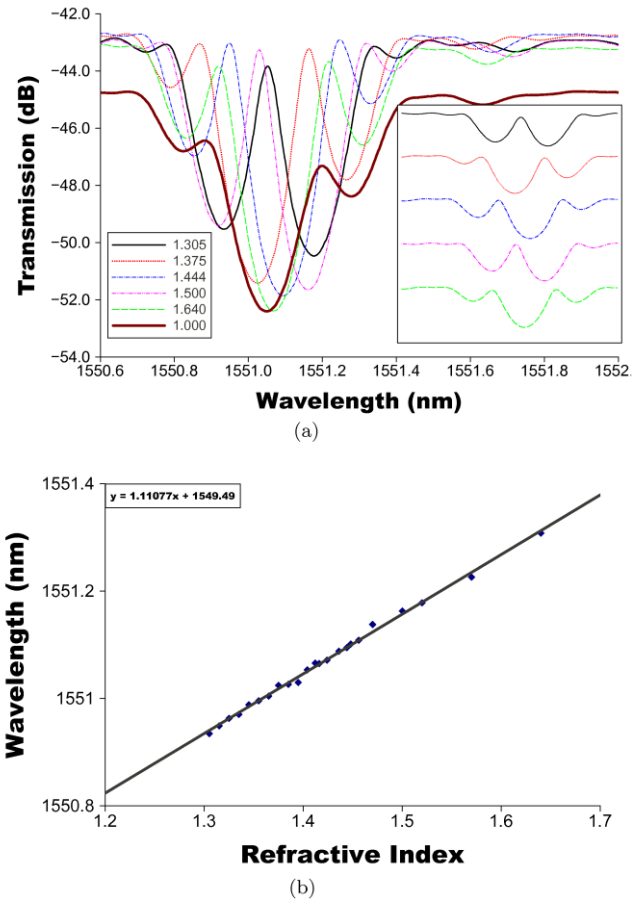

Fig. 3. (a) Spectral evolution of the 5μm microchannel device subject to different RI oils; inset shows the offset spectra. (b) Linear relation between the wavelength of the resonant peak and RI of the oil, with a coefficient of 1.1nm/RIU.

#141693 - $15.00 USD Received 25 Jan 2011; revised 11 Mar 2011; accepted 24 Mar 2011; published 2 Jun 2011

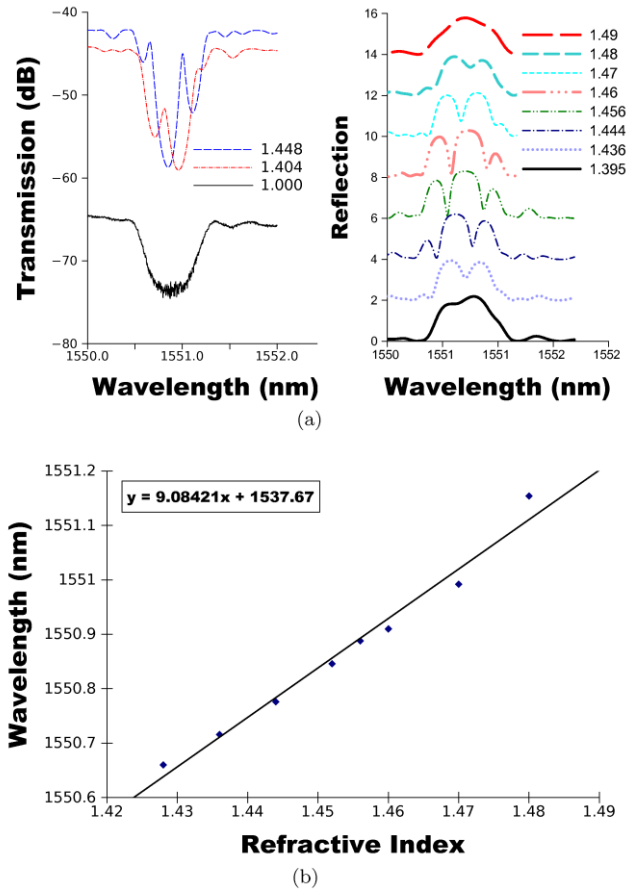

Fig. 4. (a) Spectral evolution of the 35μm microchannel device subjected to different RI oils. (b) Relation between the wavelength of the resonant peak and RI of the oil.

4. Discussion

By comparing the performance of these two microchannel FBG FP devices, we can see that the wider microchannel sample gives a much higher RI sensitivity. However, the high insertion loss limits its working range, available only from 1.39 to 1.49. On the other hand, the 5μm microchannel sample exhibits low insertion loss and works for a much broader RI sensing range from 1.3 to 1.7 but with lower sensitivity. Obviously, it is the width of the microchannel determines the sensitivity and the loss of the device. For the 5μm microchannel, only a very tiny portion (~0.5%) of the FP cavity is contributing, resulting in much lower overall effect on the structure, thus lower sensitivity and loss.

In order to design optimized microchannel FBG FP sensors, simulation was carried out to find the performance of the fabricated devices using the transfer matrix method described in Chapter 4 of [20]. Firstly, we analyzed the effect caused by the insertion loss of a microchannel. As explained in [18], microchannels with small height would yield significant insertion loss due to scattering. In our design, we created microchannel with 10μm height, which is slightly larger than the diameter of the fiber core, giving lower scattering loss. However, in real fabrication, there will be some errors causing extra loss, which can be categorized as apparent scattering loss. With light entering the microchannel, the electromagnetic field will be diffracted and higher index oil generally diffracts light less and more light will be coupled back to fiber after passing through the microchannel. With t

#141693 - $15.00 USD Received 25 Jan 2011; revised 11 Mar 2011; accepted 24 Mar 2011; published 2 Jun 2011

designated as the transmission coefficient through the microchannel for the electromagnetic field, the transfer matrix for the microchannel can be written as:

$$T_C = \begin{bmatrix} t \cdot \exp\left[\dfrac{-i2\pi nl}{\lambda}\right] & 0 \\ 0 & t^{-1} \cdot \exp\left[\dfrac{i2\pi nl}{\lambda}\right] \end{bmatrix}$$

where λ is the wavelength and n and l are the RI and length of the microchannel.

It is reasonable to assume that light propagating through a microchannel is similar to butt coupling between two fibers and we can then adopt a formula used in [21] to estimate the transmission coefficient of a microchannel as $t = \left(al^2 + 1\right)^{-1}$. For a given microchannel length which decides sensitivity of the device, we can either use a single channel with a length of L or concatenate m number of small channels and each with a length of L/m, thus the transmission can be expressed as $t = \left(a\left(L/m\right)^2 + 1\right)^{-m}$. Using approximation from Taylor series, the single channel gives $t = 1 - a \cdot L^2$, while for the concatenated channels, $t = 1 - a \cdot L^2/m$. By comparison, we can clearly see that the concatenated microchannels will give a lower insertion loss than the single channel by a factor of *m*. Taking the 5μm microchannel discussed in previous sections as the example, the loss is around 2.1dB when the channel is in air, as is given in Fig. 3(a). Seven such 5μm channels made in tandem offering a sensitivity equivalent to a single 35μm microchannel would show only 14.7dB (2.1dB × 7) loss, which is 7dB lower than the real fabricated 35μm single channel sample. Thus, it can be envisaged that by employing multiple narrower channels, such as the 1.2μm channels, a much lower insertion loss and larger RI detection range will be achieved in addition to high RI sensitivity.

The transfer matrix for a bare fiber section is similar to T_C, by omitting losses and using fiber index n' and corresponding length l', T_F is given by:

$$T_F = \begin{bmatrix} \exp\left[\dfrac{-i2\pi n'l'}{\lambda}\right] & 0 \\ 0 & \exp\left[\dfrac{i2\pi n'l'}{\lambda}\right] \end{bmatrix}$$

The transfer matrix for a uniform Bragg grating T_{FBG} is given in [20]:

$$T_{FBG} = \begin{bmatrix} a_{11} & a_{12} \\ a_{21} & a_{22} \end{bmatrix}$$

Where $a_{11} = \cosh\left(\tau L_{FBG}\right) - i \cdot \sinh\left(\tau L_{FBG}\right)$ and $a_{12} = -i \cdot \kappa/\tau \sinh\left(\tau L_{FBG}\right)$ with $\tau = \left(\kappa^2 - \sigma^2\right)^{\frac{1}{2}}$, $\kappa = \pi/\lambda \cdot \delta n_{eff}$, $\sigma = 2\pi n_{eff}/\lambda - \pi/\Lambda$ and L_{FBG} accounting for the length of the grating. Λ is the period of the grating and n_{eff} and δn_{eff} are effective index of the fiber and its perturbation in the grating, respectively. The final effective transfer matrix for a microchannel FBG FP structure is then given by:

$$T_{FBG} \cdot T_F \cdot T_C \cdot T_{FBG}$$

#141693 - $15.00 USD Received 25 Jan 2011; revised 11 Mar 2011; accepted 24 Mar 2011; published 2 Jun 2011

Here, we assume the two FBGs are identical. By examining T_F and T_C, we can notice that $T_F \cdot T_C = T_C \cdot T_F$, which hints that the relative position of the microchannel in the cavity would not influence the optical properties of the device. Figure 5 gives the simulated transmission spectra for different t for an FBG FP with a 35μm microchannel in the cavity. Apparently, smaller t corresponds to larger loss. In the simulation, we use two uniform FBGs of 4000 periods with Λ = 0.532nm and $\delta n = 10^{-4}$ and they are separated by 1mm. As can be observed in Fig. 5, when $t = 1$ the spectrum shows clear resonances and a low insertion loss, while with decreasing of t, visibility of the resonances gradually drops and overall insertion loss increases. This trend agrees very well with the experimental results for the 35μm microchannel device we observed.

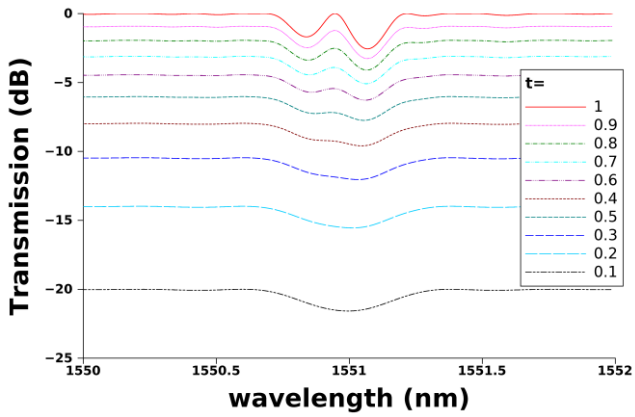

Fig. 5. Simulated transmission spectra for a microchannel FBG FP cavity with different transmission coefficients.

We also tracked the generation of the resonant peaks in the spectrum by varying the oil index n in T_C (with t = 1) and the results are plotted in Figs. 6(a) and 6(b). We clearly see from the figure that each peak appears in the short wavelength side initially and moves to longer wavelength with increasing RI, behaving like a propagating wave till it moving out of the Bragg reflection band. All resonant peaks show a linear RI response with a sensitivity of ~10nm/RUI, which is very close to the measured sensitivity of the real device, as shown by the green triangle points on the same figure. Similarly, for the device with a 5μm wide channel, our simulated results showed a resonant peak sensitivity of 1.4nm/RUI, which is again in good agreement with experimental result (1.1nm/RIU).

We further examined the influence by the FBG FP cavity length and the simulation results are shown in Fig. 6(b). Clearly, for both narrow and broad microchannels, shorter FP cavity length gives rise to higher RI sensitivity. This offers another design parameter to optimize the structure and function of the proposed microchannel FBG FP sensors.

#141693 - $15.00 USD Received 25 Jan 2011; revised 11 Mar 2011; accepted 24 Mar 2011; published 2 Jun 2011

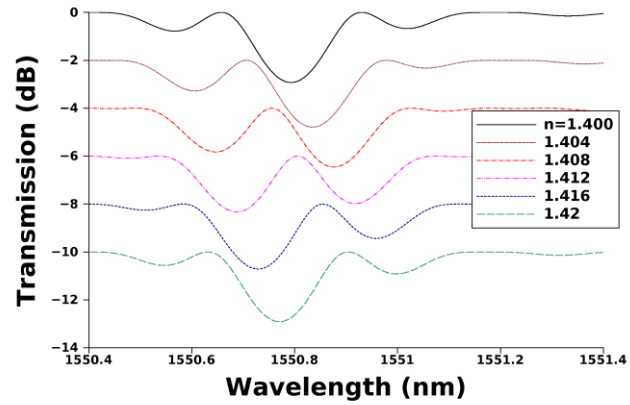

(a)

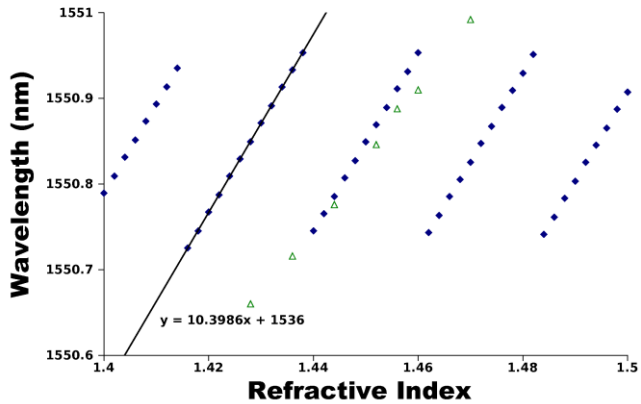

(b)

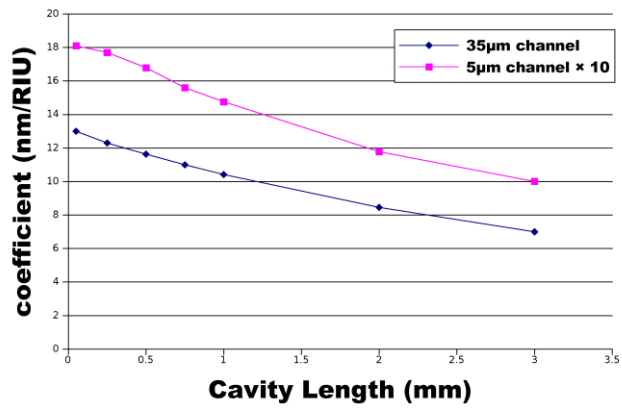

(c)

Fig. 6. (a)Simulated spectra of the 35μm device with oils of different RI in the microchannel. (b) Wavelength shift of the FP resonance peaks with respect to RI of the oil; the triangles are the experimental result for comparison. (b) Influence on RI sensitivity of a microchannel FBG FP device with different cavity lengths.

#141693 - $15.00 USD Received 25 Jan 2011; revised 11 Mar 2011; accepted 24 Mar 2011; published 2 Jun 2011

5. Conclusion

In this paper, we have described a new type of RI sensors based on an FBG FP cavity embedded with a microchannel. Microchannels with different sizes have been realized using fs laser inscription assisted chemical etching and the narrowest width of only 1.2μm has been demonstrated. Two FBG FP structures with a relatively narrow (5μm) and broad (35μm) channel were used for RI sensing characterization, showing a linear RI response with sensitivities of 1.1nm/RIU and 9nm/RIU, respectively. The broader channel device gives considerable high loss and can work only in a limited RI range from 1.43 to 1.49. In contrast, the narrow channel device gives a much larger RI measurement range from 1.3 to 1.7. We also performed a theoretical simulation by employing transfer matrix technique and the simulation results are in excellent agreement with experimental ones. More importantly, the modeling has revealed the influence of the device parameters and structure on loss and RI sensitivity, which provides a good design tool for optimized sensors. Overall, the revealed linear RI response with significantly larger detection range and high sensitivity of the microchannel FBG FP sensors are of great advantages over fiber grating based refractometers, as the latter all have a nonlinear RI response with detection range limited to fiber core index only to 1.44. With these remarkable advantages, microchannel FBG FP structures could be further developed into high performance bio/chemical/environmental sensors.

#141693 - $15.00 USD Received 25 Jan 2011; revised 11 Mar 2011; accepted 24 Mar 2011; published 2 Jun 2011